Supplementary Information

A Stimuli-Responsive Nanopore Based on a Photoresponsive Host-Guest System

Yi-Lun Ying, Junji Zhang, Fu-Na Meng, Chan Cao, Xuyang Yao, Itamar Willner, He Tian and Yi-Tao Long

Contents

Single-channel *I-V* curves of α-HL

Supplementary Figure S10

The blockage currents for irreversible inhibitions treated with the repulsive potential

Supplementary Figure S11

^{1}H NMR spectra (400MHz, D_2O, 298K) changes of V^{2+}-*trans*-Az after complexation with SC_4

Supplementary Figure S12

^{1}H NMR spectra (400MHz, D_2O, 298K) changes of V^{+} after complexation with SC_4

Supplementary Figure S13

τ_{on} histograms for the inhibitions of α-HL in the presence of the host-guest complex in the *trans* compartment at the holding potential of -140 mV

Supplementary Figure S14

^{1}H NMR spectra (400MHz, D_2O, 298K) of V^{2+}-*trans*-Az and isomerization from V^{2+}-*trans*-Az to V^{2+}-*cis*-Az after irradiation

Supplementary Figure S15

^{1}H NMR spectra (400MHz, D_2O, 298K) of isomerization from SC_4:V^{2+}-*trans*-Az to SC_4:V^{2+}-*cis*-Az after irradiation for 30 min

Supplementary Figure S16

The current traces recording at the holding potential of -100 mV with and without UV irradiation

Supplementary Figure S17

UV-*vis* spectra for the photoisomerization of SC_4:V^{2+}-Az

Supplementary Figure S18

^{1}H-NMR spectra (400MHz, D_2O, 298K) of SC_4, V^{2+}-*trans*-Az and SC_4: V^{2+}-*trans*-Az

Supplementary Figure S19

^{13}C-NMR spectrum (400MHz, DMSO-d_6, 298K) of V^{2+}-*trans*-Az

Supplementary Figure S20

ESI-MS spectrum of V^{2+}-*trans*-Az

Supplementary Figure S21

^{1}H-NMR spectrum (400MHz, D_2O, 298K) of V^{+}

1. The close-states of *α*-hemolysin induced by *para*-sulfonato-calix[4]arene

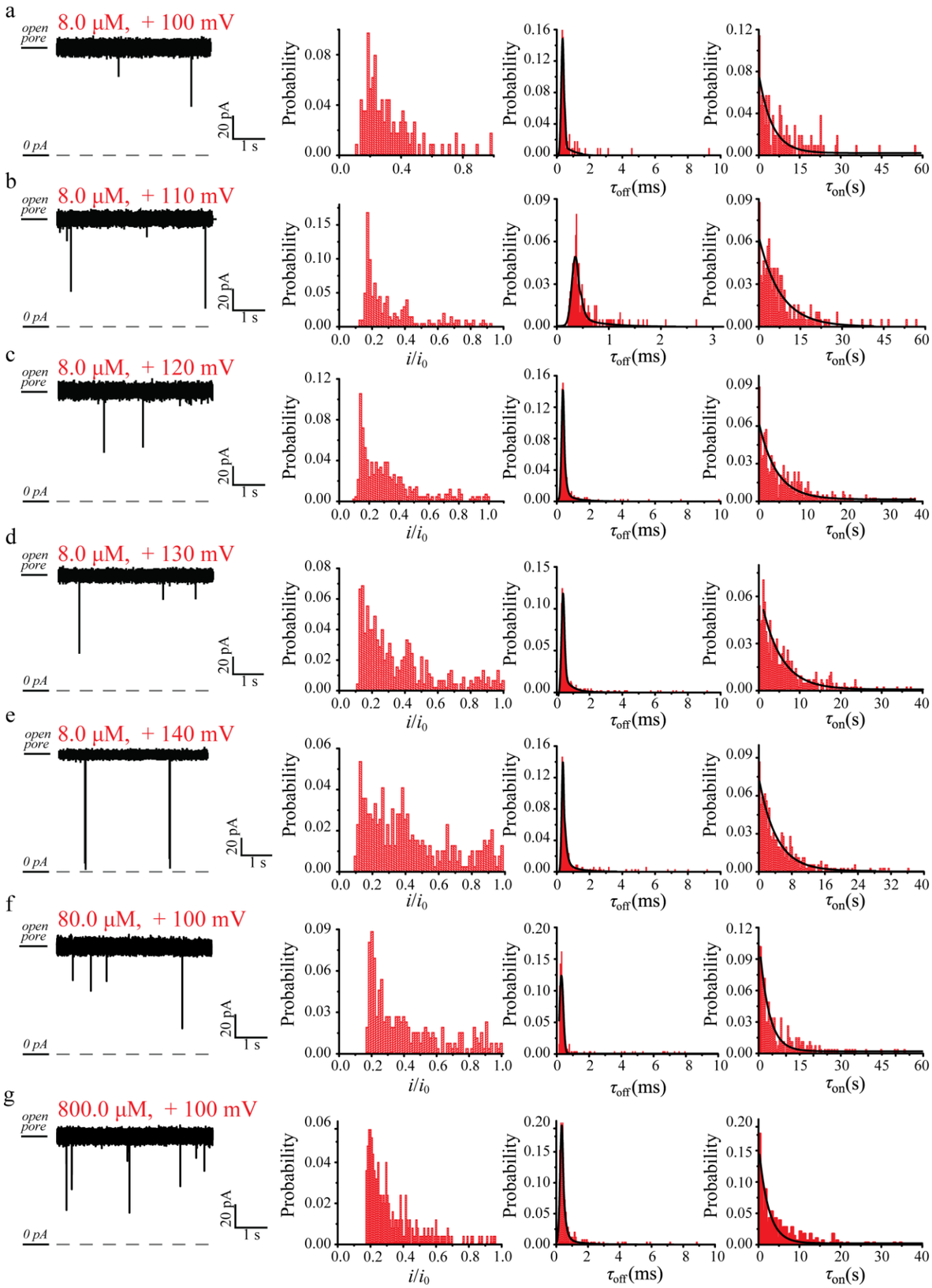

Supplementary Figure S1 | The raw data, current histograms, τ_{off} histograms and τ_{on} histograms for the blockages

by adding the varied concentrations of SC_4 into the *cis* compartment at different holding potentials (V_h). (**a**) [SC_4] = 8.0 μM, V_h = + 100 mV, (**b**) [SC_4] = 8.0 μM, V_h = + 110 mV, (**c**) [SC_4] = 8.0 μM, V_h = +120 mV, (**d**) [SC_4] = 8.0 μM, V_h = +130 mV, (**e**) [SC_4] = 8.0 μM, V_h = +140 mV, (**f**) [SC_4] = 80.0 μM. V_h = +100 mV and (**g**) [SC_4] = 800.0 μM. V_h = +100 mV. The transient and reversible close-states were retained even at an extreme holding potential of +140 mV. The curves of the τ_{off} histograms for the concentration of SC_4 at 8.0 μM follow a relatively steep rise and fall, but for times greater than the peak values are well approximated by single-exponential decays. For the concentration of SC_4 at 80.0 μM and 800.0 μM, Gaussian distributions of durations were observed. τ_{on} histograms are approximated by single-exponential decays.

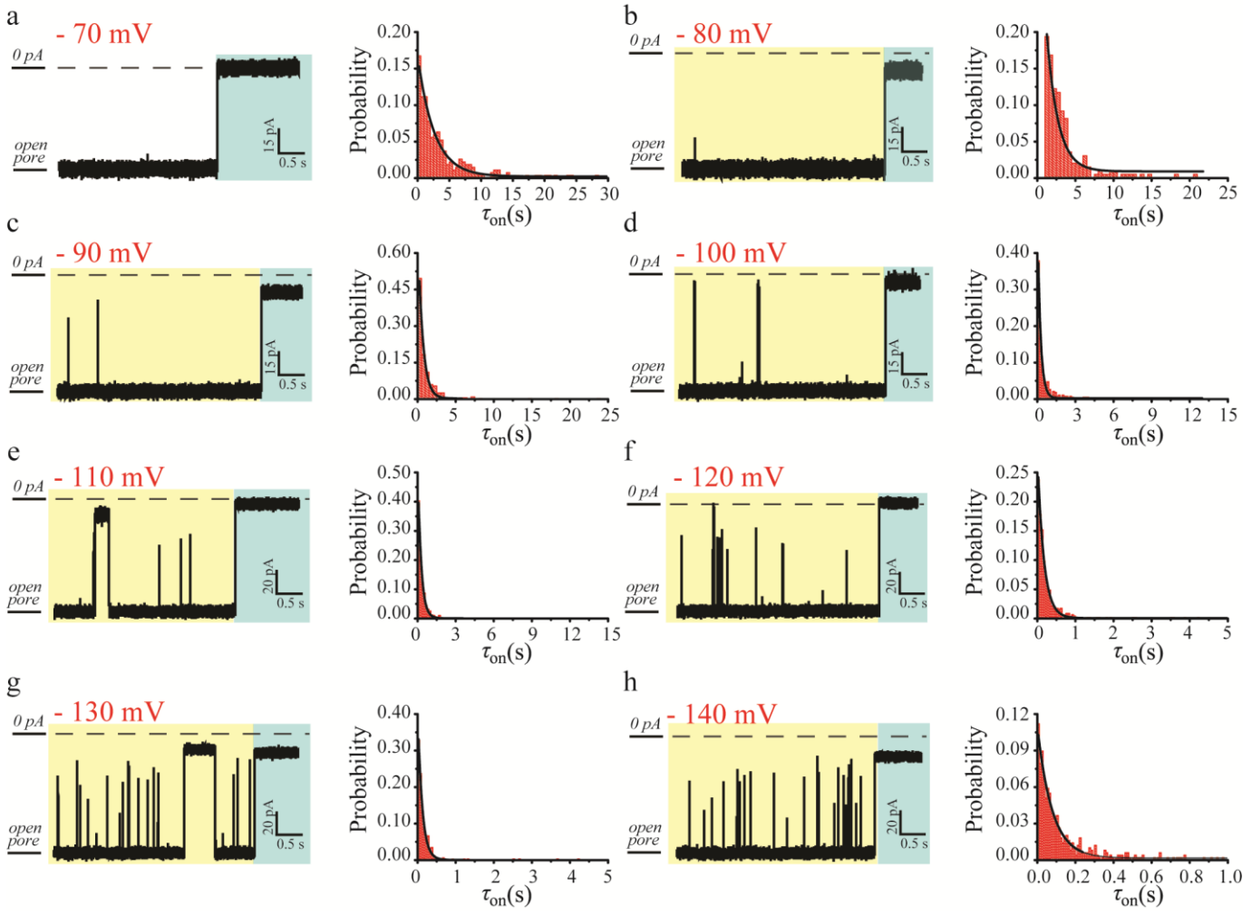

Supplementary Figure S2 | The raw data and τ_{on} histograms for the inhibitions of α-HL induced by the addition of SC_4 (8.0 μM) into the *trans* compartment at different holding potentials: (**a**) -70 mV, (**b**) -80 mV, (**c**) -90 mV, (**d**) -100 mV, (**e**) -110 mV, (**f**) -120 mV, (**g**) -130 mV and (**h**) -140 mV. Yellow and blue rectangle boxes represent the reversible and irreversible inhibitions, respectively. τ_{on} histograms are approximated by single-exponential decays.

Supplementary Table S1 | The fitted parameters of SC_4 induced inhibitions from the *cis* side.

[SC_4] (μM)	Potential (mV)	τ_{on} [a] (s)	$\tau_{off\text{-}1}$ [b] (ms)	$\tau_{off\text{-}2}$ [b] (ms)
8.0	+100	4.86 ± 0.50	0.36 ± 0.01	0.58 ± 0.02
8.0	+110	4.45 ± 1.10	0.36 ± 0.02	0.51 ± 0.03
8.0	+120	4.35 ± 0.42	0.38 ± 0.02	0.79 ± 0.04
8.0	+130	4.79 ± 0.50	0.38 ± 0.03	0.51 ± 0.02
8.0	+140	4.26 ± 0.38	0.37 ± 0.02	0.78 ± 0.03
80.0	+100	4.76 ± 0.47	0.34 ± 0.02	n.a.
800.0	+100	4.75 ± 0.53	0.34 ± 0.02	n.a.

[a] The values of τ_{on} are carried out for all the events including reversible and irreversible inhibitions, and obtained by single-exponential fittings. [b] The values of $\tau_{off\text{-}1}$ and $\tau_{off\text{-}2}$ for *cis* side inhibitions at [SC_4] = 8.0 μM are fitted by Gaussian functions following by single-exponential equations. The durations for *cis* side inhibitions at [SC_4] = 80.0 μM and 800.0 μM are fitted by Gaussian functions. Data of the values were based on three separate experiments.

Supplementary Table S2 | The fitted parameters of SC_4 induced inhibitions from the *trans* side.

[SC_4] (μM)	Potential (mV)	τ_{on} [a] (s)	$\tau_{off\text{-}1}$ [b] (ms)	$\tau_{off\text{-}2}$ [b] (ms)	$\tau_{off\text{-}PI}$ [c] (ms)
8.0	-70	2.61 ± 0.70	0.30 ± 0.04	n.a.	0.28 ± 0.04
8.0	-80	1.49 ± 0.50	0.32 ± 0.03	n.a.	0.28 ± 0.05
8.0	-90	0.62 ± 0.32	0.30 ± 0.02	2.62 ± 0.28	0.23 ± 0.05
8.0	-100	0.49 ± 0.24	0.37 ± 0.03	2.92 ± 0.30	0.31 ± 0.04
8.0	-110	0.27 ± 0.15	0.60 ± 0.04	3.18 ± 0.31	0.29 ± 0.05
8.0	-120	0.17 ± 0.07	0.35 ± 0.02	2.64 ± 0.35	0.36 ± 0.05
8.0	-130	0.12 ± 0.04	0.43 ± 0.03	3.02 ± 0.32	0.35 ± 0.04
8.0	-140	0.07 ± 0.02	0.36 ± 0.04	3.51 ± 0.34	0.25 ± 0.05
0.8	-100	8.14 ± 0.75	0.34 ± 0.75	n.a.	0.28 ± 0.03
4.0	-100	2.01 ± 0.24	0.38 ± 0.34	n.a.	0.26 ± 0.04

[a] The values of τ_{on} were carried out for all the events including reversible and irreversible inhibitions. The values of τ_{on} are obtained by single-exponential fittings. [b] The values of $\tau_{off\text{-}1}$ and $\tau_{off\text{-}2}$ for *trans* side reversible inhibitions are calculated by di-exponential decays at the holding potentials ranging from -90 mV to -140 mV with the concentration of SC_4 at 8.0 μM. The histograms for the duration time of the reversible inhibitions at the holding potentials of -70 mV and -80 mV with [SC_4] = 8.0 μM are fitted by the single-exponential equations giving the values of $\tau_{off\text{-}1}$. The values of $\tau_{off\text{-}1}$ for the concentration of SC_4 at 0.8 μM and 4.0 μM are obtained by single-exponential equations. [c] The values of $\tau_{off\text{-}PI}$ representing duration time of the reversible events at PI are fitted by single-exponential equations. Data of the values were based on three separate experiments. Since the values of $\tau_{off\text{-}PI}$ are close to the values of $\tau_{off\text{-}1}$, $\tau_{off\text{-}2}$ represent the fitted long duration time for the inhibitions in PII and PIII.

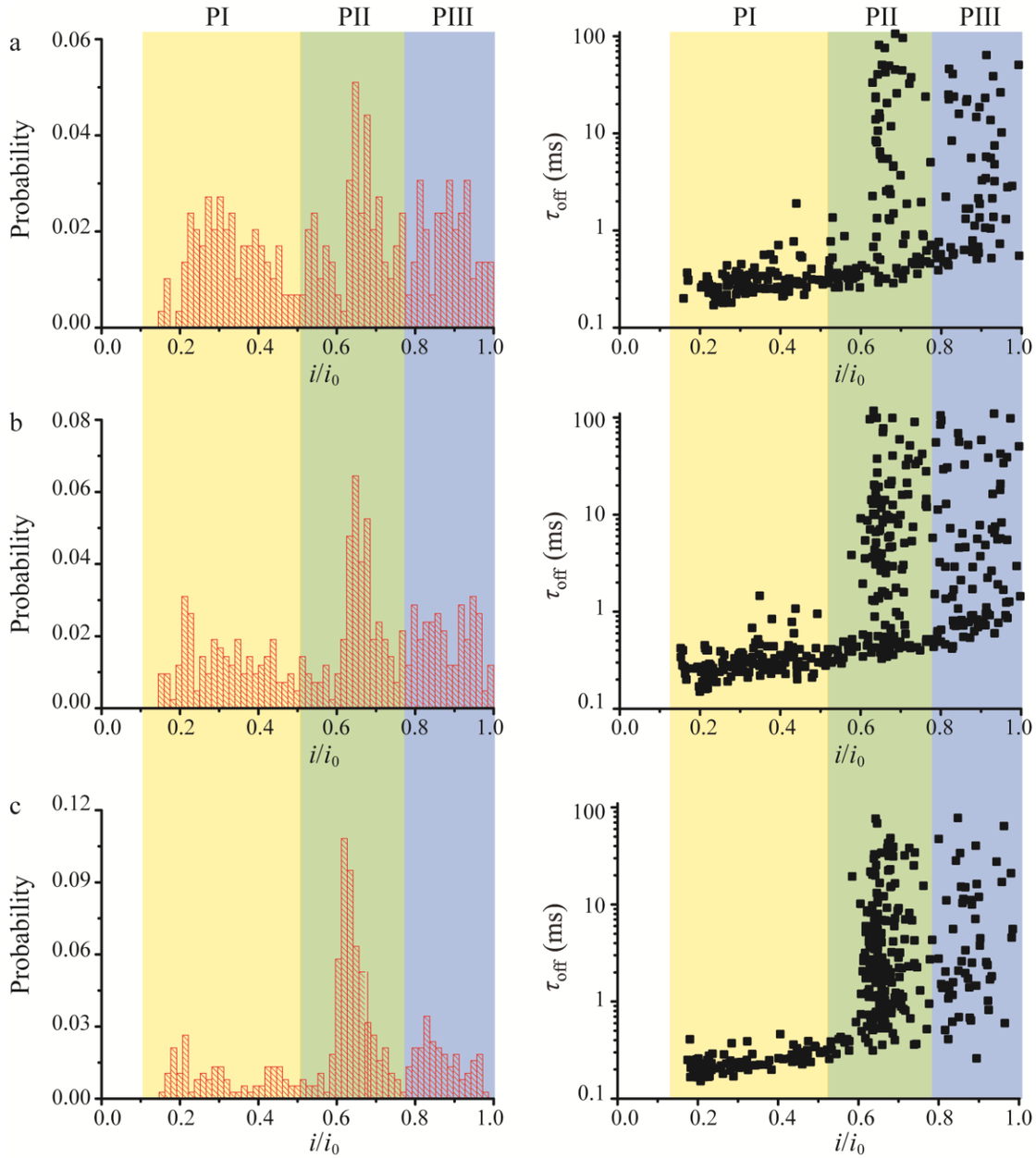

Supplementary Figure S3 | Histograms of the *trans* side inhibition currents and the scatter plots of reversible *trans* side inhibitions at different potentials: (**a**) -70 mV, (**b**) -80 mV and (**c**) -90 mV. The inhibitions fall into three populations which are assigned to PI, PII and PIII, respectively. The ratios for the events in PI from the total events are 0.55, 0.34, 0.22 at the potential of -70 mV, -80 mV and – 90 mV, respectively. The histograms of the inhibition currents include reversible and irreversible inhibitions.

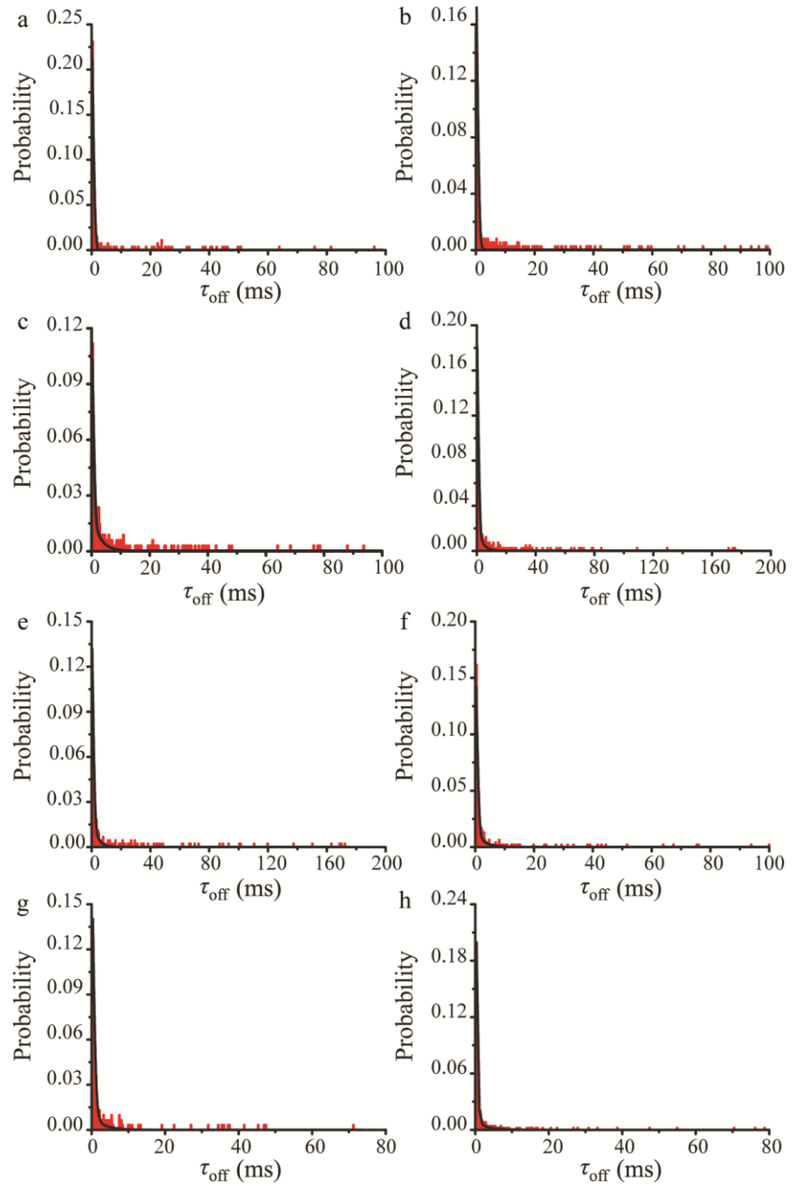

Supplementary Figure S4 | The τ_{off} histograms for the reversible inhibitions of α-HL induced by the addition of SC_4 (8.0 μM) into the *trans* compartment at different holding potentials: (**a**) -70 mV, (**b**) -80 mV, (**c**) -90 mV, (**d**) -100 mV, (**e**) -110 mV, (**f**) -120 mV, (**g**) -130 mV and (**h**) -140 mV. The τ_{off} histograms for holding potentials at -70 mV and -80 mV are fitted by single-exponential decays. The histograms of reversible inhibitions for the *trans* side assays are fitted by double-exponential equations at holding potentials ranging from -90 mV to -140 mV.

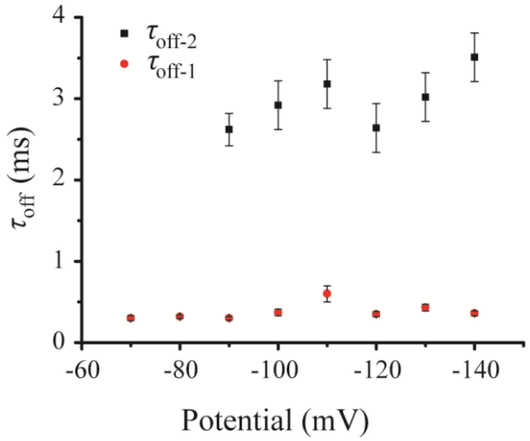

Supplementary Figure S5 | Plots of τ_{off} versus the applied potential changing at intervals of 10 mV in the presence of SC_4 at the *trans* compartment. The plot of τ_{off-1} is down in red and the plot of τ_{off-2} is up in black. Since α-HL consists of an assembly of seven monomers, the periodic change of τ_{off-2} with the increased negative holding potential might be caused by the inhibitions at different binding ratio. Other factors including the protonation of the residues in α-HL and simultaneous multiple bindings may affect the relationship between τ_{off-2} and the applied potential, which needs further studies.

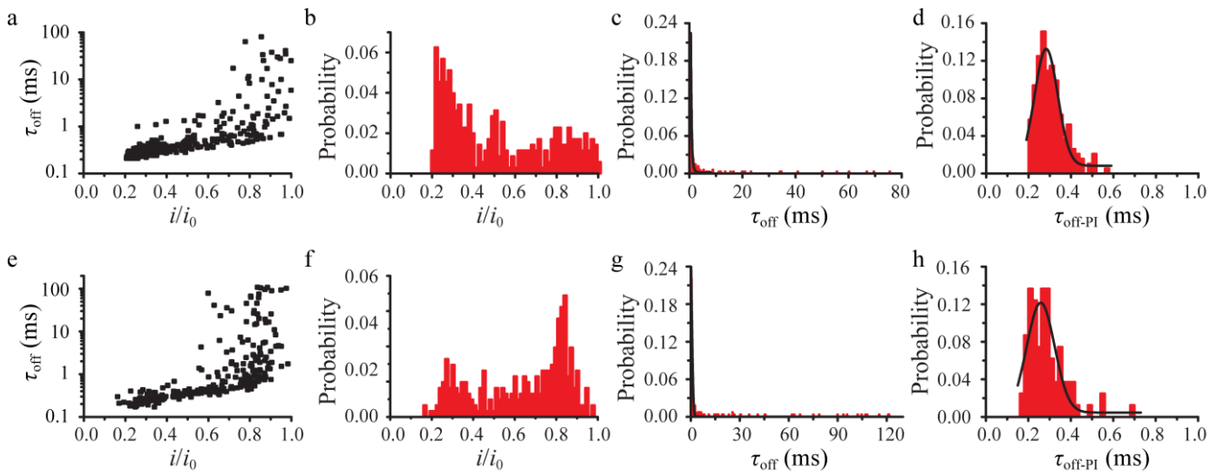

Supplementary Figure S6 | The scatter plots, current distributions, τ_{off} histograms and τ_{off-PI} histograms for the *trans* side inhibitions of α-HL at the holding potential of -100 mV in the presence of different concentrations of SC_4: (**a**) ~ (**d**) 0.8 μM, (**e**) ~ (**h**) 4 μM. τ_{off} histograms are approximated by single-exponential decays. The curves of the durations in PI are fitted by Gaussian functions. The ratios for the events in PI from the total events are 0.58 and 0.30 for the concentrations of SC_4 at 0.8 and 4.0 μM, respectively.

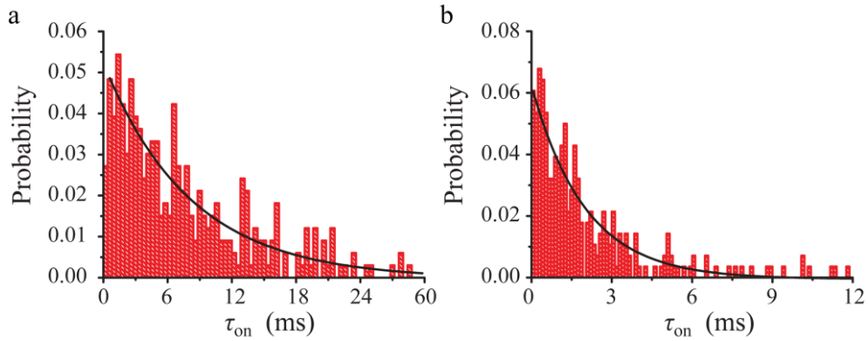

Supplementary Figure S7 | The τ_{on} histograms for the *trans* side inhibitions of *α*-HL at the holding potential of -100 mV in the presence of different concentrations of SC_4: (**a**) 0.8 μM, (**b**) 4 μM. τ_{on} histograms are approximated by single-exponential decays.

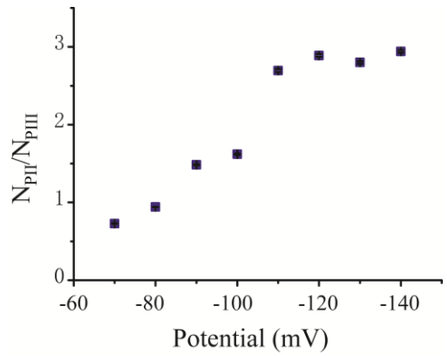

Supplementary Figure S8 | Plots of N_{PII}/N_{PIII} versus the applied potential changing at intervals of 10 mV in the presence of 8.0 μM SC_4 at the *trans* compartment. The counts of events in PII and PIII were based on the Gaussian distributions of current histograms.

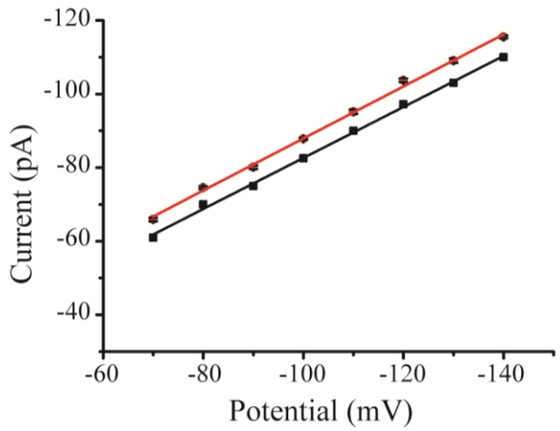

Supplementary Figure S9 | Single-channel *I-V* curves of *α*-HL. *I-V* curves before (black) and after addition of SC_4 into the *trans* compartment in 3000 s (red).

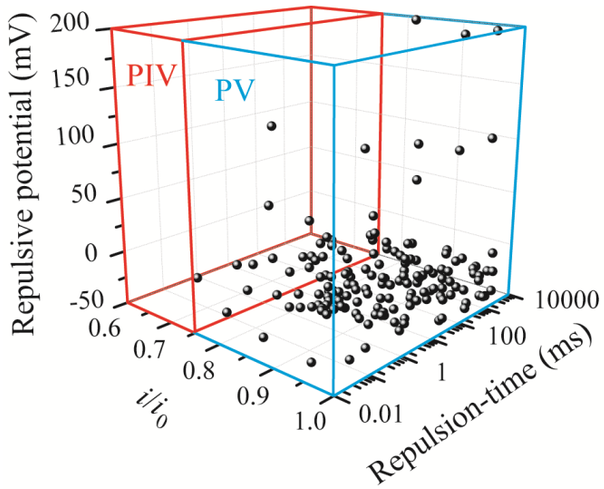

Supplementary Figure S10 | The blockage currents for irreversible inhibitions at the holding potential from -70 mV to -140 mV, treated with the repulsive potential. SC_4 would be relieved from the α-HL after undergoing the certain repulsion-time. The irreversible inhibitions are divided into two populations PIV and PV. It should be noted that the close-states with the higher inhibition currents exhibit more positive repulsive potentials and higher values of repulsion-time as PIV, and vice versa as PV.

2. Binding behavior between SC_4 and V^{2+}-*trans*-Az

The formation of the inclusion complex between SC_4 and guest molecule V^{2+}-*trans*-Az is evident in ^1H NMR spectroscopic experiment in D_2O (Supplementary Fig. S11). In the presence of SC_4, all the protons of V^{2+}-*trans*-Az exhibit a visible upfield shift (Δδ) owing to the ring current effect of the aromatic nuclei, which suggests that the V^{2+}-*trans*-Az guest is encapsulated into the cavity of SC_4. However, the Δδ value for each proton is different, which can be used as a powerful evidence to deduce the host-guest binding manner.[47] As can be seen from Supplementary Fig. S10, protons on the methyl group of pyridinium (g) perform the most significant upfield shift from δ = 4.37 ppm to δ = 1.58 ppm after complexation, while protons on the methylene group (c, from δ = 5.90 to δ = 5.78) and acetyl methyl group (f, from δ = 2.26 to δ = 2.24) hardly change their places. Supplementary Figure S11 shows the chemical shift of hydrogens on the viologen and azobenzene moieties. The proton a-H, which is adjacent to pyridinium methyl group, shifts significantly to upfield, from δ = 8.93 to δ = 6.62. The proton b-H shows a relatively mild upfield shift from δ = 8.40 to δ = 7.40. Compared to the protons a-H and b-H, their counterparts on the other pyridinium part of viologen moiety (a'-H and b'-H) show only minute upfield shift (b'-H from δ = 9.10 to δ = 8.90; a'-H from δ = 8.46 to δ = 8.11) while protons on the azobenzene moiety (d-H, d'-H, e-H and e'-H) stay the same. The Δδ value of V^{2+}-*trans*-Az protons are in the order of CH_3(pyri, g-H)>a-H>b-H>>b'-H>a'-H>other protons, which indicates that V^{2+}-*trans*-Az is immersed into the cavity of SC_4 in its axial orientation with the methyl group being included first. The electrostatic interactions contribute favorably to the binding affinity between SC_4 and V^{2+}-*trans*-Az. In neutral (or the basic) solution, some of the phenolic hydroxyls of

calixarenes begin to be deprotonated.[51] Therefore, the electron-rich cavities of calixarenes are capable of providing π-stacking interaction. In the research of Liu et al.[47], SC_4 shows the π-stacking interaction towards the methyl viologen (MV^{2+}) besides the electrostatic interactions at the pH = 7.2. Thus, the π-stacking interactions exist between SC_4 and V^{2+}-*trans*-Az besides the major effect of electrostatic interactions.

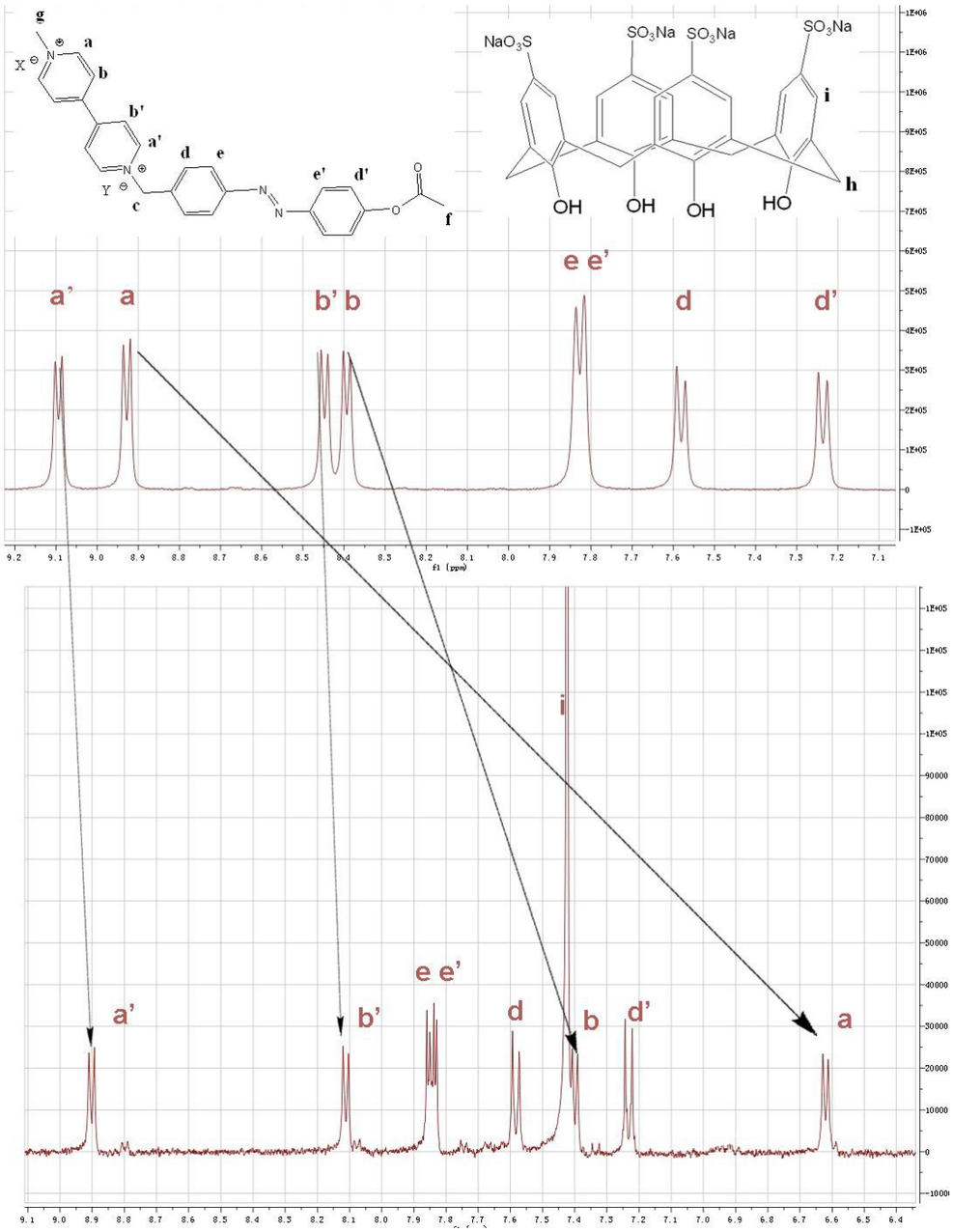

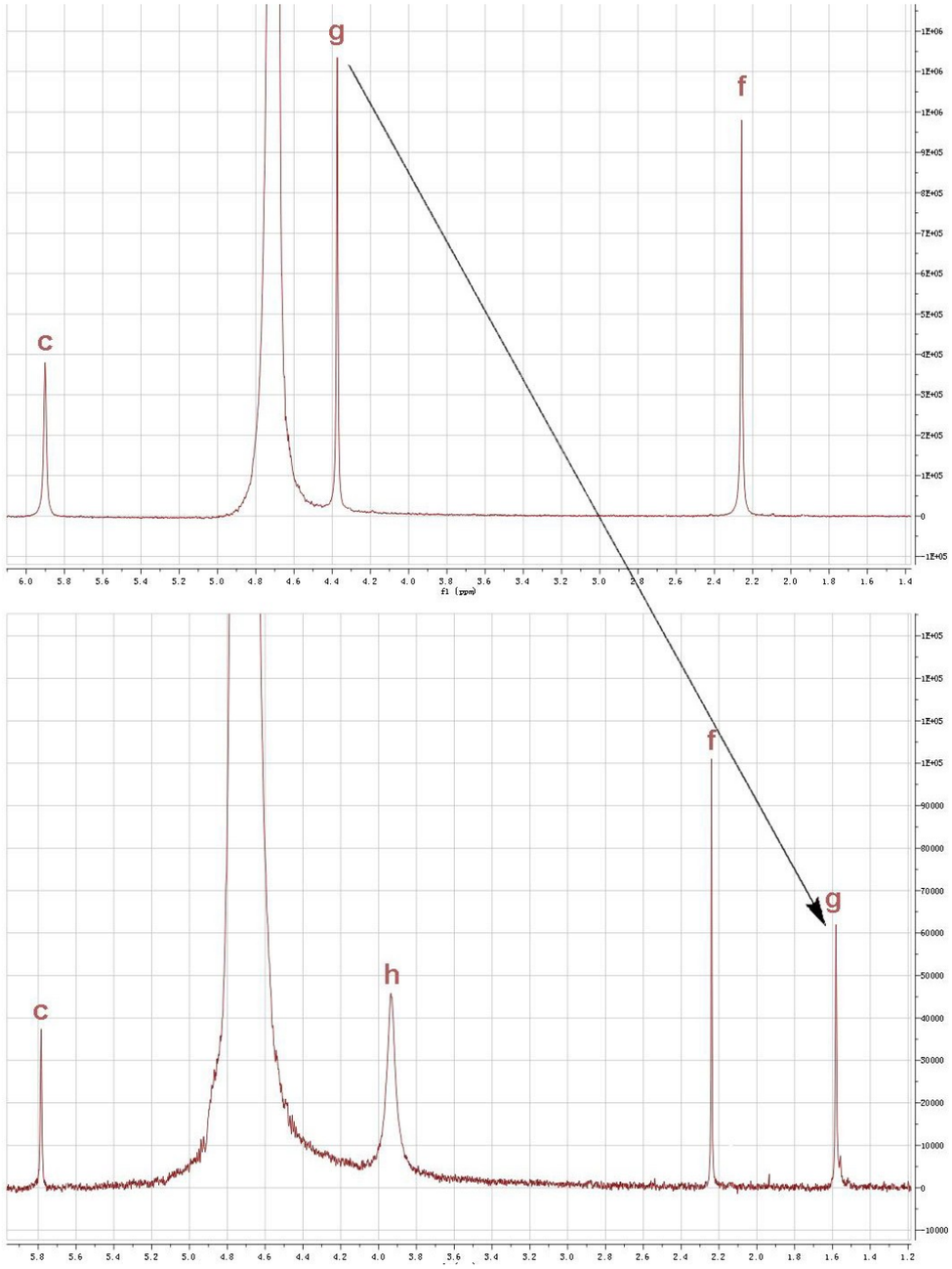

Supplementary Figure S11 | ^{1}H NMR spectra (400MHz, D_2O, 298K) changes of V^{2+}-*trans*-Az after complexation with SC_4.

The information of inclusion complexe between SC_4 and control guest molecules V^{+} is evident in ^{1}H NMR spectroscopic experiment in D_2O (Supplementary Fig. S12). In the presence of SC_4, all the protons of guest molecule exhibit a visible upfield shift(Δδ) due to the ring current effect of the aromatic nuclei, which suggests that the V^{+} is encapsulated into the cavity of SC_4. However, the Δδ value for each proton is different, which can be used as a powerful evidence to deduce the host-guest binding manner. As can be seen from Supplementary Fig. S12 (bottom), protons on the methyl group of

pyridinium (c) perform the most significant upfield shift from δ=4.28 ppm to δ=1.36 ppm after complexation. Supplementary Fig. S12 (top) shows the chemical shift of hydrogens on the viologen moiety. The proton a'-H shifts significantly to upfiled from δ=8.62 ppm to δ=7.64 ppm. The proton b'-H also shows a notable upfield shift from δ=7.76 ppm to δ=6.70 ppm. Compared to the protons a'-H and b'-H, their counterparts on the other pyridinium part of viologen moiety (a-H and b-H) show only minute upfield shift (a-H from δ=8.75 to δ=8.70; b-H from δ=8.23 to δ=8.04). The Δδ value of V^+ protons are in order of CH_3(pyri,c-H)>b'-H>a'-H>b-H>a-H, which indicates that V^+ is immersed into the cavity of SC_4 in its axial orientation with the methyl pyridinium part being included first.

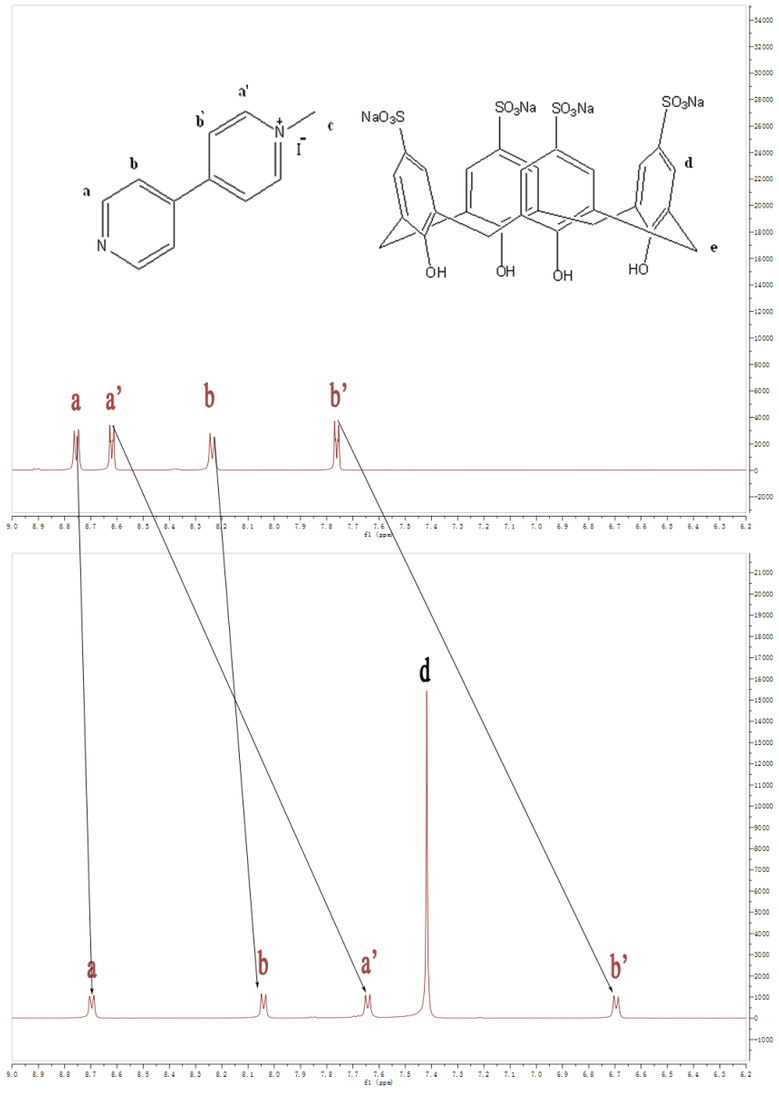

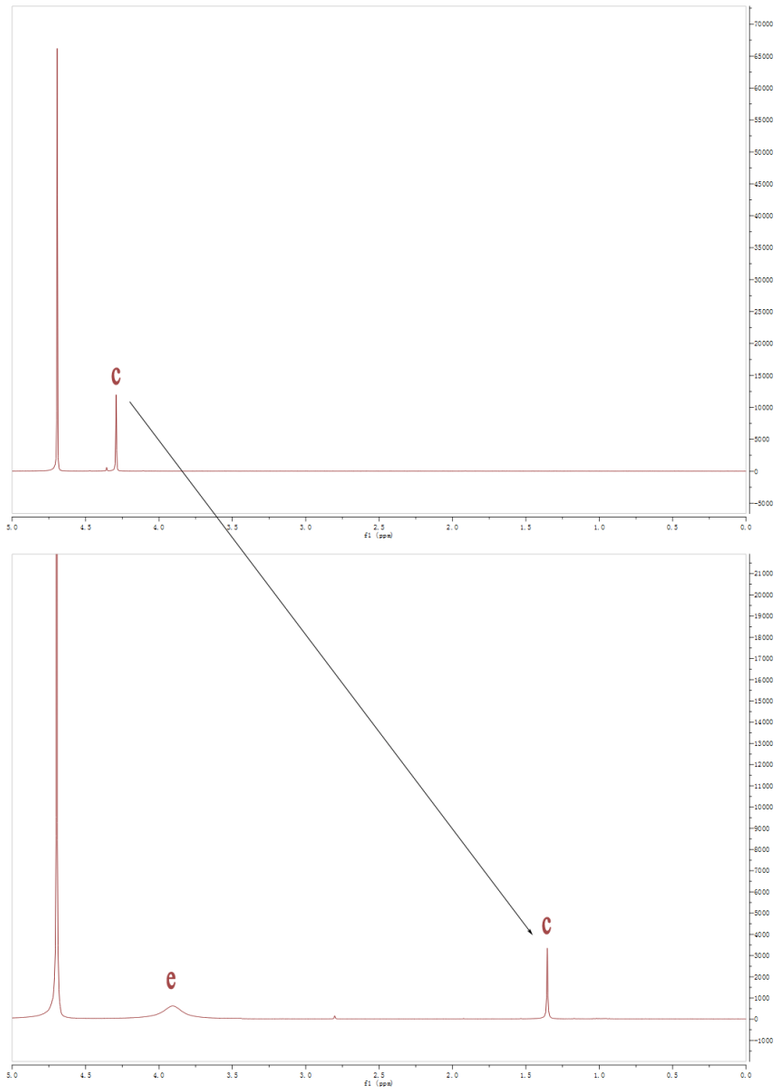

Supplementary Figure S12 | ^{1}H NMR spectra (400MHz, D_2O, 298K) changes of V^+ after complexation with SC_4.

3. Recognition of host-guest interactions through an *α*-HL

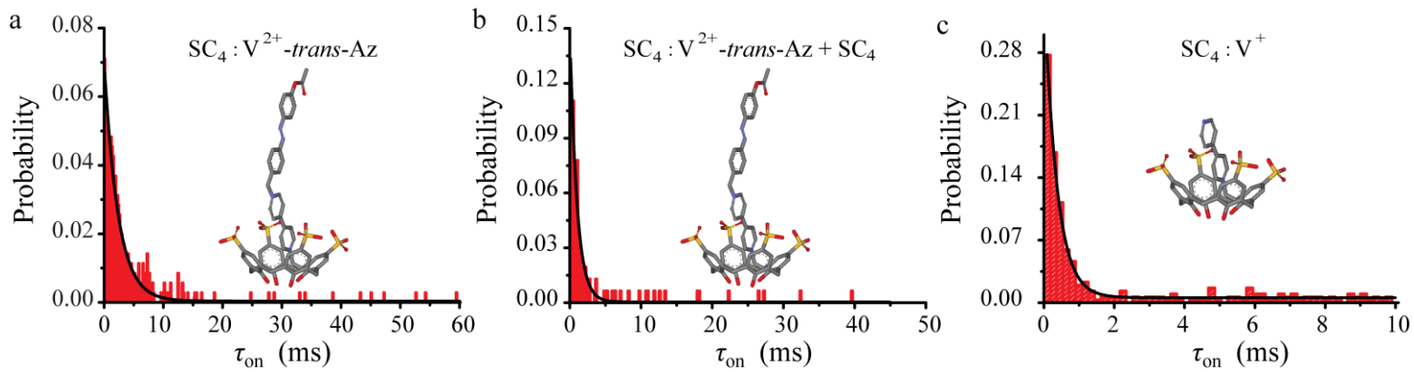

Supplementary Figure S13 | τ_{on} histograms for the inhibitions of *α*-HL in the presence of the host-guest complex in

the *trans* compartment at the holding potential of -140 mV: (**a**) SC_4:V^{2+}-*trans*-Az, (**b**) SC_4:V^{2+}-*trans*-Az with the addition of 1.6 μM SC_4 and (**c**) SC_4:V^{+}. The single-exponential decays are used to fit the τ_{on} histograms.

4. Binding behaviors between SC_4 and V^{2+}-*trans*-Az/ V^{2+}-*cis*-Az

As shown in Supplementary Fig. S14, the irradiation of V^{2+}-*trans*-Az with UV light (λ=365 nm) for 30 min results in ^{1}H NMR spectra changes attributed to the formation of V^{2+}-*cis*-Az. The protons on the azobenzene moiety show partial upfield shifts owing to the isomerization of *trans*-azobenzene to its *cis* form. The most affected protons are e-H and e'-H which sit on the ortho-position of azo bond. New bands appear at δ = 6.95-7.00 of *cis* isomer compared to δ = 7.82/7.84 (Δδ = ca.0.9) of the *trans* isomer. The protons on the meta-position of azo group, d-H and d'-H, also reveal a distinct partial shift from δ = 7.61/7.24 (*trans*) to δ = 7.37/6.92 (*cis*). Moderate upfield shift can also be observed in methylene protons (c-H) as well as acetyl methyl protons (f-H). New peaks arise in δ = 5.79 (c-H, *cis*)/ δ = 2.18 (f-H, *cis*) compared to δ = 5.94 (c-H, *trans*)/ δ = 2.28 (f-H, *cis*) before irradiation. However, protons on viologen moiety are hardly affected by the isomerization of azobenzene. Only a'-H, which is the most adjacent proton to azobenzene group, shows a minute and partial upfield shift from δ = 9.11 (*trans*) to δ = 9.02 (*cis*). These results demonstrate that the isomerization of azobenzene does not affect the chemical environment of protons on the viologen moiety which interact with SC_4.

The ^{1}H NMR spectra of complex SC_4:V^{2+}-*trans*-Az before (top) and after (bottom) irradiation for 30 min (λ = 365 nm) are represented in Supplementary Fig. S15. One can notice that protons on the viologen moiety also show partial chemical shifts. New peaks appear on δ = 8.84 (*cis* a'-H), δ = 8.14 (*cis* b'-H), δ = 6.64 (*cis* a-H), compared to δ = 8.95 (*trans* a'-H), δ = 8.18 (*trans* b'-H), δ = 6.68 (*trans* a-H), respectively. b-H is unfortunately overlapped with protons on SC_4 (i-H), and thus can not be analyzed. Even the protons on the viologen methyl group, which is the complexation site with SC_4 and the most distant group from the azobenzene moiety, show a partial chemical shift from δ = 1.58 (*trans*) to δ = 1.55 (*cis*). As mentioned above, the isomerization of azobenzene would not affect the chemical shifts of protons on viologen moiety except the most adjacent a'-H (Supplementary Fig. S14). Therefore, the chemical shifts of protons on viologen group associated with SC_4 indicate a chemical environment change in the complex which is probably due to the perturbation of interaction between V^{2+}-*cis*-Az and SC_4 through the variation of dipole moment during the isomerization.

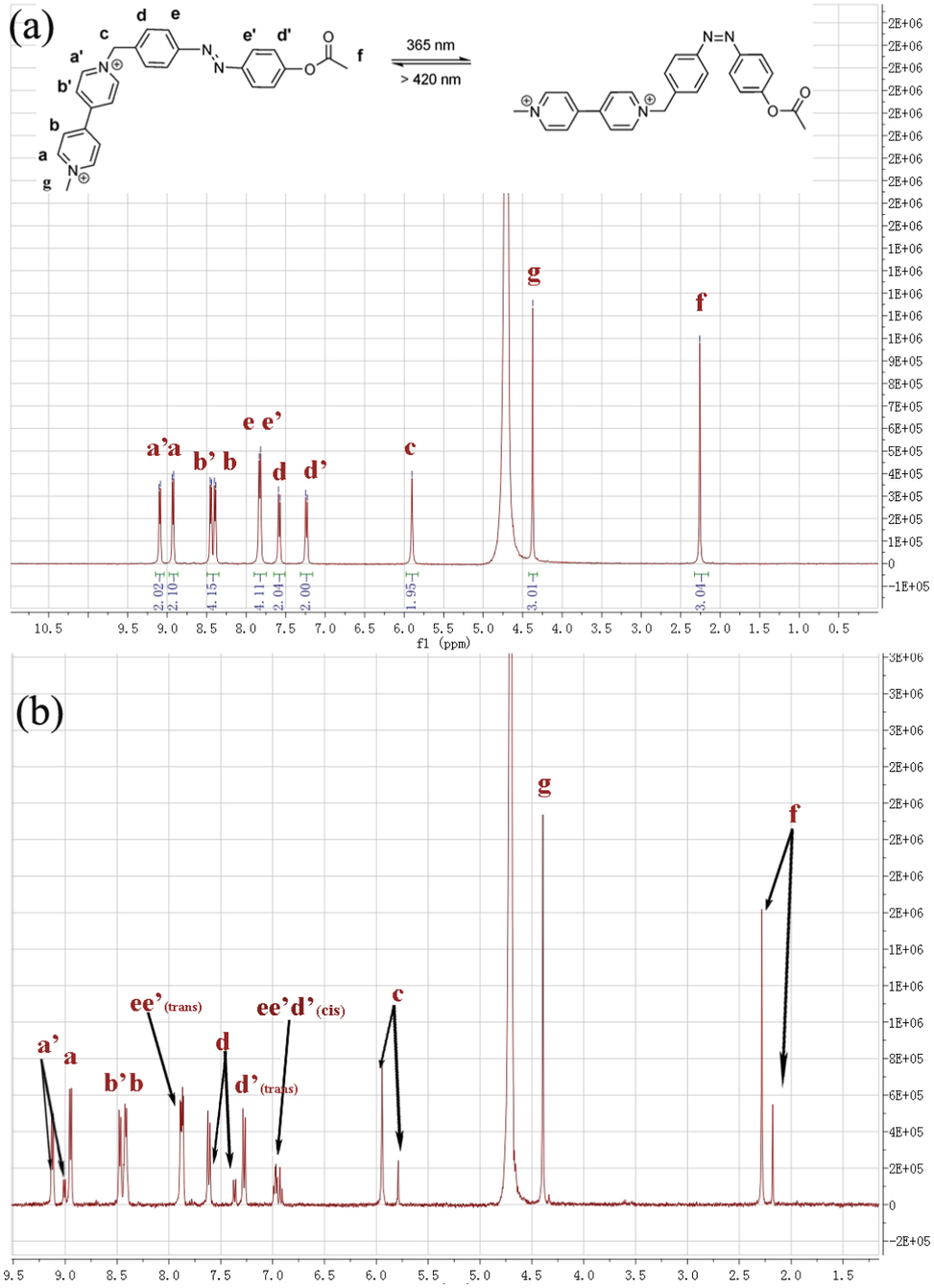

Supplementary Figure S14 | ^{1}H NMR spectra (400MHz, D_2O, 298K) of V^{2+}-*trans*-Az and isomerization from V^{2+}-*trans*-Az to V^{2+}-*cis*-Az after irradiation. (**a**) ^{1}H NMR spectrum of V^{2+}-*trans*-Az and (**b**) ^{1}H NMR spectrum of V^{2+}-*trans*-Az after irradiation.

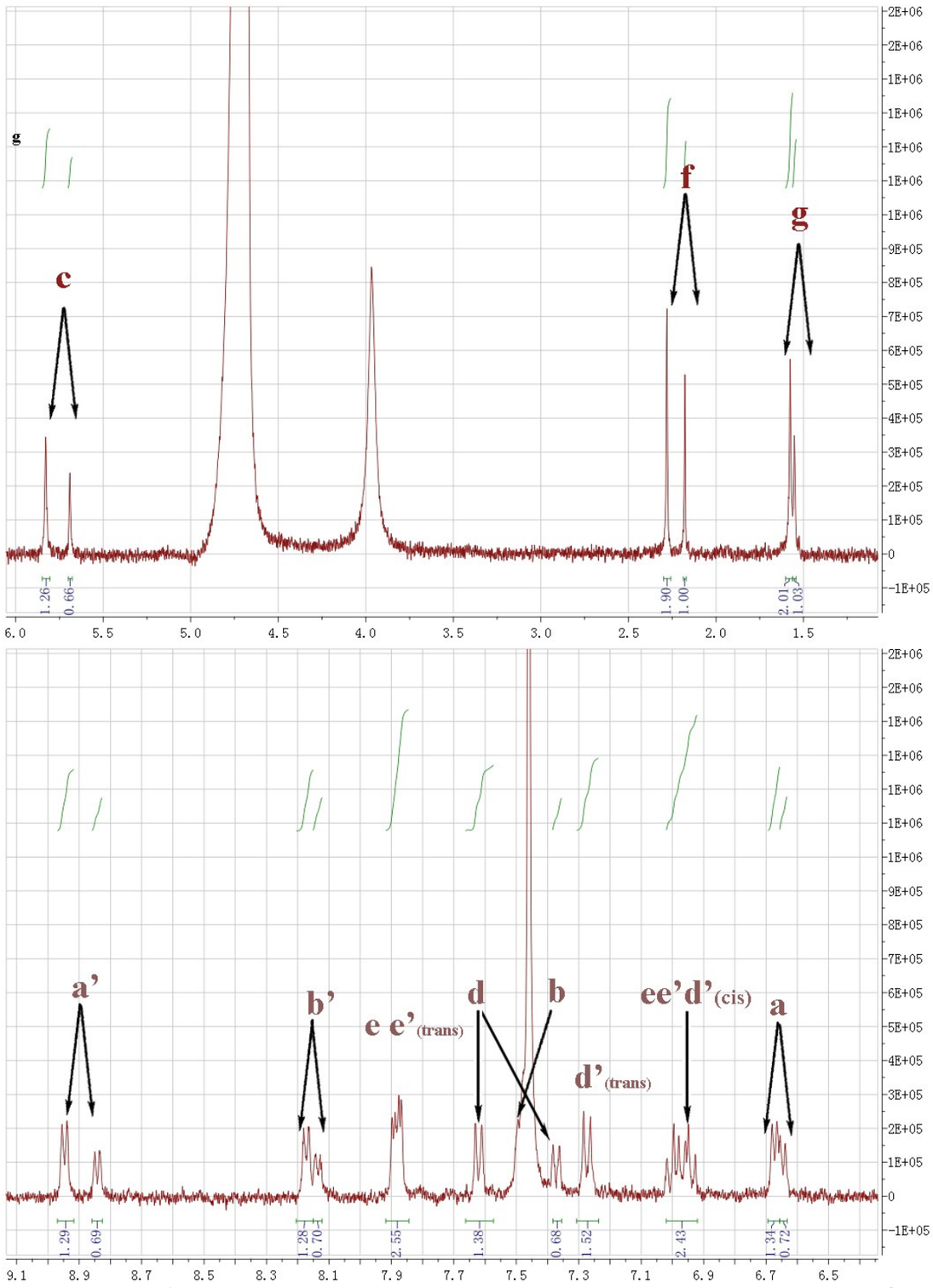

Supplementary Figure S15 | ^{1}H NMR spectra (400MHz, D_2O, 298K) of isomerization from SC_4:V^{2+}-*trans*-Az to SC_4:V^{2+}-*cis*-Az after irradiation for 30 min.

5. Real-time monitoring a light-induced molecular machine by an *α*-HL: SC_4 system

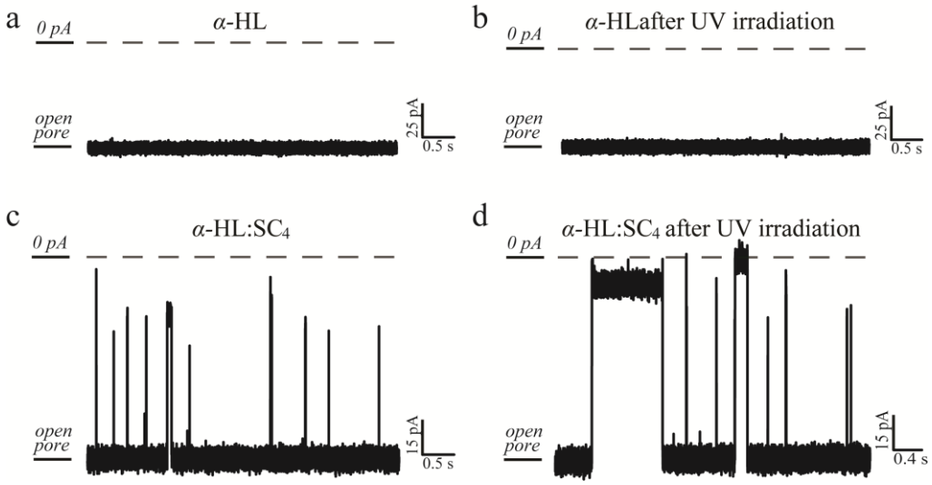

Supplementary Figure S16 | The current traces recording at the holding potential of -100 mV: (**a**) *α*-HL, (**b**) *α*-HL after 2400 s UV irradiation, (**c**) *α*-HL:SC_4 system, (**d**) *α*-HL:SC_4 system after 2400 s UV irradiation. *α*-HL:SC_4 system was formed by adding 8.0 μM SC_4 into the *trans* compartment.

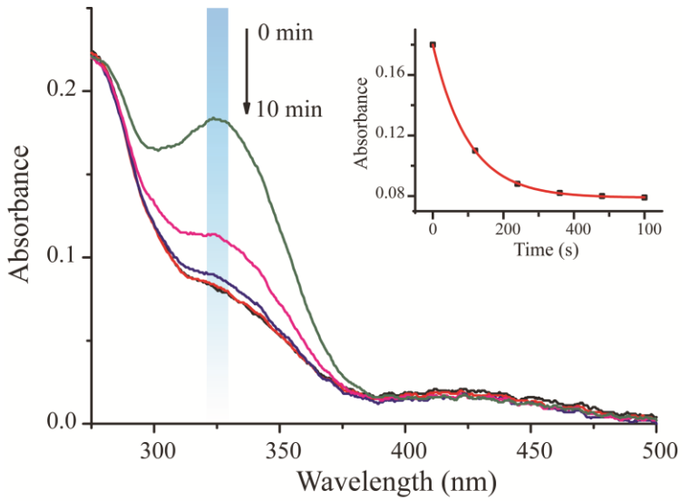

Supplementary Figure S17 | UV-*vis* spectra for the photoisomerization of SC_4:V^{2+}-Az. Insert: Exponential time dependence of the changes in the UV-Vis absorption at λ = 325 nm of SC_4:V^{2+}-Az. The decay constant (*τ*) is 101 s.

6. **Synthesis procedure**

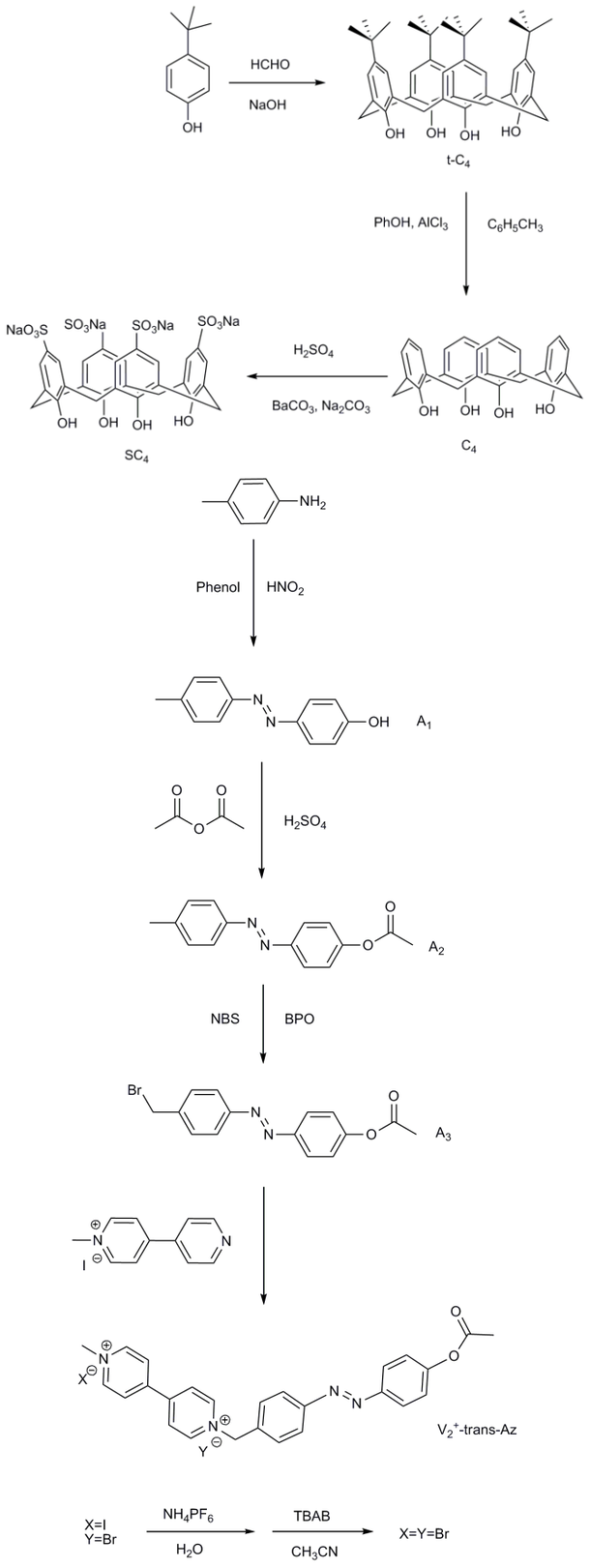

***p* -tert-Butylcalix[4]arene or 5,11,17,23-Tetrakis(*tert*butyl)-25,26,27,28-tetrakis(hydroxy)calix[4]arene [t-C_4]**[52]

A mixture of 31 mL (1.2 mol) of 37% formaldehyde was added to 50 g (0.3 mol) *p-tert*-butyl phenol in a 1 L three-necked round-bottom flask. NaOH (1.2 mL, 0.09 mmol) (40% solution in H_2O) was added to the mixture. The flask was stirred uncovered at 20 °C for 15 min and then was heated to 120 °C for 2 h under a steady flow of N_2. As H_2O was removed, the clear solution turned from yellow to dark yellow. After 2.5 h, some frothing occurred, and the solution became more viscous. Stirring was continued until the yellow to amber viscous material did not stick to the side of the flask. The cooled very viscous solid was dissolved in 500 mL of diphenyl ether in 30 min. The dissolved solution was heated to 120 °C while N_2 was bubbled into the reaction mixture to facilitate the removal of H_2O. After about 1 h, the solution was brought to reflux (ca. 350 °C), and the flask was fitted with a condenser. After 3 h the color of the solution changed from yellow to clear dark brown. A crude white precipitation (33.5 g, 62%) was obtained upon addition of EtOAc to the cooled reaction mixture and was filtered and washed, successively, with EtOAc (2 × 50 mL), acetic acid (100 mL), H_2O (2 × 50 mL), and acetone (2 × 25 mL). Recrystallization from toluene yielded 31.1 g (50.8%) of [t-C4] as gleaming white crystals. ^{1}H NMR spectra were recorded on a Brüker AM 400 spectrometer with tetramethyl silane (TMS) as internal reference. MS were recorded on EI or ESI mass spectroscopy. ^{1}H NMR (400 MHz, $CDCl_3$, 298K): δ 10.36 (s, 4H), δ 7.05 (s, 8H), 4.25 (d, J = 12.6 Hz, 4H), 3.51 (d, J = 12.6 Hz, 4H), 1.21 (s, 36H).

25,26,27,28-Tetrakis(hydroxy)calix[4]arene [C_4][53]

A slurry of 15.0 g (22.5 mmol) of *p-tert*-butylcalix[4]arene [t-C_4], 10.2g (108 mmol) of phenol, and 15.8 g (118 mmol) of $AlCl_3$ was stirred in 125 mL of toluene at 20 °C for 1 h under N_2. The mixture was poured into 250 mL of 0.2 N HCl, the organic phase was separated, and the solvent was evaporated. Upon addition of MeOH the precipitate formed was filtered to give 8.5 g of a solid. The crude product was recrystallized from MeOH/$CHCl_3$ to afford colorless crystals (7.4 g, 73%). ^{1}H NMR (400 MHz, $CDCl_3$, 298K): δ 10.20 (s, 4H), 7.05 (d, J = 7.6 Hz, 8H), 6.73 (t, J = 7.6 Hz, 4H), 4.26 (s, 1H), 3.51 (d, J = 23.9 Hz, 1H).

***p* -sulfonatocalix[4]arene or 5,11,17,23-Tetrakis(sulfonato)-25,26,27,28-tetrakis(hydroxy)calix[4]arene [SC_4]**[54]

[C_4] (1.0 g, 2.4 mmol) was mixed with concentrated H_2SO_4 (10 ml) and the solution was heated at 60 °C for 4 h. An aliquot was withdrawn from the reaction mixture and poured into water. The reaction was completed when no water-insoluble material was detected in the aliquot. After cooling, the precipitate was filtered off through a glass filter. The precipitate was dissolved in water and the aqueous solution was neutralised by $BaCO_3$. The precipitation was filtered off and washed with hot water and the combined filtrate and washings were evaporated to dryness under reduced pressure. The residue was dissolved in hot water (15 ml) and the solution was adjusted to pH 8 by Na_2CO_3. After filtration, methanol was added to the filtrate to afford a white precipitate (1.55g, 80%). ^{1}H NMR (400 MHz, D_2O, 298K) δ 7.49 (s, 8H), 3.92 (s, 8H).

4-hydroxyl-4'-methyl-azobenzene (A1)[52]

$NaNO_2$ (52.25 g, 0.61 mol) dissolved in 387.5 mL H_2O, was added dropwise into *p*-toluidine (80 g, 0.75mol) mixed with 225 mL HCl (36.5%) at 0 ~ 5°C. The final solution was kept stirring at 0°C for 15 min. Then a mixture of phenol (72 g, 0.76 mol) and 125 mL water was added dropwise into the above solution at 0 ~ 5 °C. The reaction was carried out at this temperature overnight and then NaOH was added until pH of 7–8 was achieved. A great deal of orange solid was gradually crystallized from the solution. The solid was filtered, washed with 700 mL CCl_4, dried in vacuo, and then gave

out orange compound **A1** (87 g, 55%). ^{1}H NMR (400 MHz, $CDCl_3$, 298K): δ 7.86 (d, *J* = 8.4 Hz, 2H), 7.79 (d, *J* = 8.4 Hz, 2H), 7.30 (d, *J* = 8.0 Hz, 2H), 6.94 (d, *J* = 8.8 Hz, 2H), 5.35 (s, 1H), 2.43 (s, 3H).

4-acetoxy-4'-methyl-azobenzene (A2)[52]

A stirred mixture of **A1** (20 g, 94.3 mmol) and conc. sulfuric acid (0.4 ml) dissolved into acetic anhydride(125 ml) was heated to 100 ºC for 3 h under argon, cooled and poured into ice water (700 ml) slowly with stirring. The solid was filtered and dried in vacuo. Thus gave out orange compound **A2** (20.8 g, 86.7%). ^{1}H NMR (400 MHz, $CDCl_3$, 298K): δ 7.94 (d, *J* = 8.4 Hz, 2H), 7.82 (d, *J* = 8.4 Hz, 2H), 7.32 (d, *J* = 8.4 Hz, 2H), 7.25 (d, *J* = 8.8 Hz, 2H), 2.45 (s, 3H), 2.35 (s, 3H).

4-acetoxy-4'-bromomethyl-azobenzene (A3)[52]

A mixture of **A2** (10.4 g, 40.9 mmol), NBS (7.7 g, 43.3 mmol), BPO (0.6 g, 2.4 mmol) and CCl_4 (211 ml) were refluxed for 12 h under an atmosphere of Ar gas. The resulting solution was filtered while it was hot. The filtrate was cooling down to 0 °C to afford orange precipitate. The precipitate was filtered, washed with CCl_4 and gave pure **A3** (10.7 g, 78.6%). ^{1}H NMR (400 MHz, $CDCl_3$, 298K): δ 7.96 (d, *J* = 8.4 Hz, 2H), 7.89 (d, *J* = 8.0 Hz, 2H), 7.55 (d, *J* = 8.0 Hz, 2H), 7.26 (d, *J* = 8.4 Hz, 2H), 4.56 (s, 2H), 2.35 (s, 3H).

Guest Molecule N-methyl dipyridium (V^+)

4,4'-dipyridine (5 g, 32.05 mmol) and methyl iodide (1.52g, 10.68 mmol) was dissolved in 50 ml acetonitrile and refluxed for 5h. After cooling to room temperature, precipitates were collected and washed with cold acetonitrile (5 ml). The products were dried under vacuo and yielded 2.8 g (85%). ^{1}H NMR (400 MHz, D_2O) δ 8.76 (d, J = 6.7 Hz, 1H), 8.62 (dd, J = 4.7, 1.6 Hz, 1H), 8.24 (d, J = 6.7 Hz, 1H), 7.76 (dd, J = 4.7, 1.6 Hz, 1H), 4.29 (s, 1H).

Guest Molecule V^{2+}-*trans*-Az[52]

1-methyl-4,4'-bipyridin-1-ium iodide (0.45 g, 1.5 mmol) was dissolved in acetonitrile (20 mL) at 70 °C. **A3** (1.5 g, 4.5 mmol) was added into the solution and the mixture was stirred at 70 °C for overnight. After cooling to room temperature, the mixture was filtered. And then the solid was washed with CH_2Cl_2 and gave a brown compound ca. 0.87g. This compound was dissolved in water (100 mL) and NH_4PF_6 (10 equiv.) was added to precipitate a yellow solid. This solid was again dissolved in acetonitrile (150 mL) and TBAB (10 equiv.) was added to precipitate an orange solid. The solid was dried in vacuo and afford pure V^{2+}-*trans*-Az (0.55 g, 62.8%). ^{1}H NMR (400 MHz, D_2O, 298K): δ 9.09 (d, *J* = 6.6 Hz, 2H), 8.93 (d, *J* = 6.7 Hz, 2H), 8.42 (dd, *J* = 21.6, 6.6 Hz, 4H), 7.83 (d, *J* = 7.9 Hz, 4H), 7.58 (d, *J* = 8.3 Hz, 2H), 7.24 (d, *J* = 8.5 Hz, 2H), 5.90 (s, 2H), 4.37 (s, 3H), 2.26 (s, 3H). ^{13}C NMR (400 MHz, DMSO-d6, 298K): δ = 168.96, 153.04, 152.19, 149.42, 149.19, 148.10, 146.58, 145.90, 137.08, 130.23, 127.10, 126.19, 123.95, 123.14, 123.02, 62.68, 48.01, 20.89. MS (ESI): m/z: 424.2 $[V^{2+}$-*trans*-Az−2Br$]^+$.

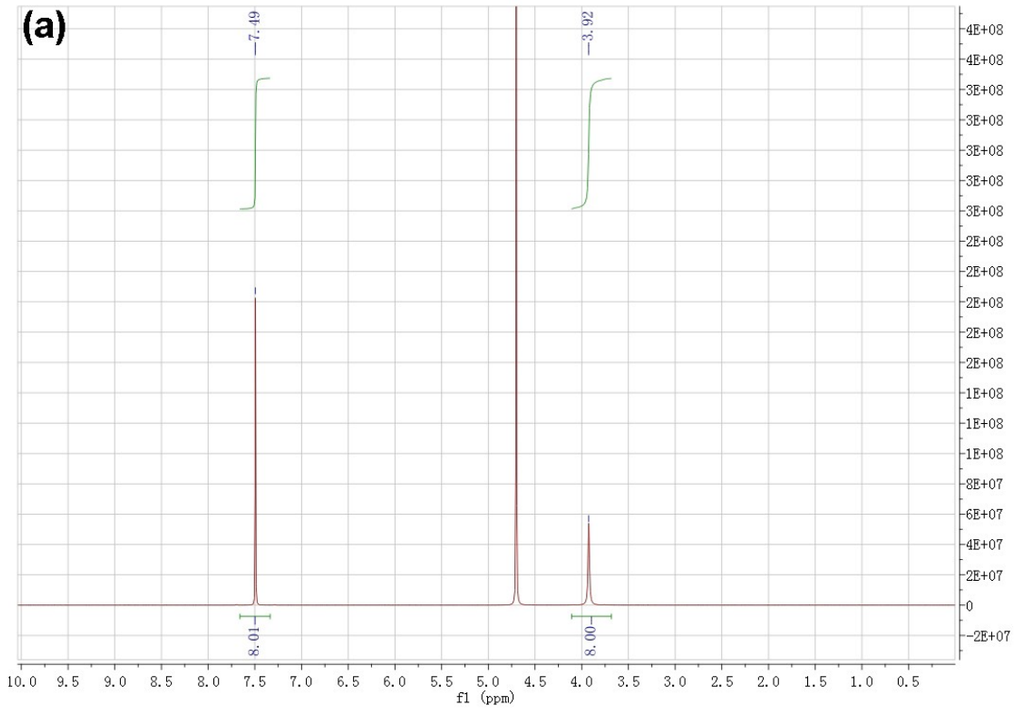
(a)
7.49
3.92
8.01
8.00
f1 (ppm)

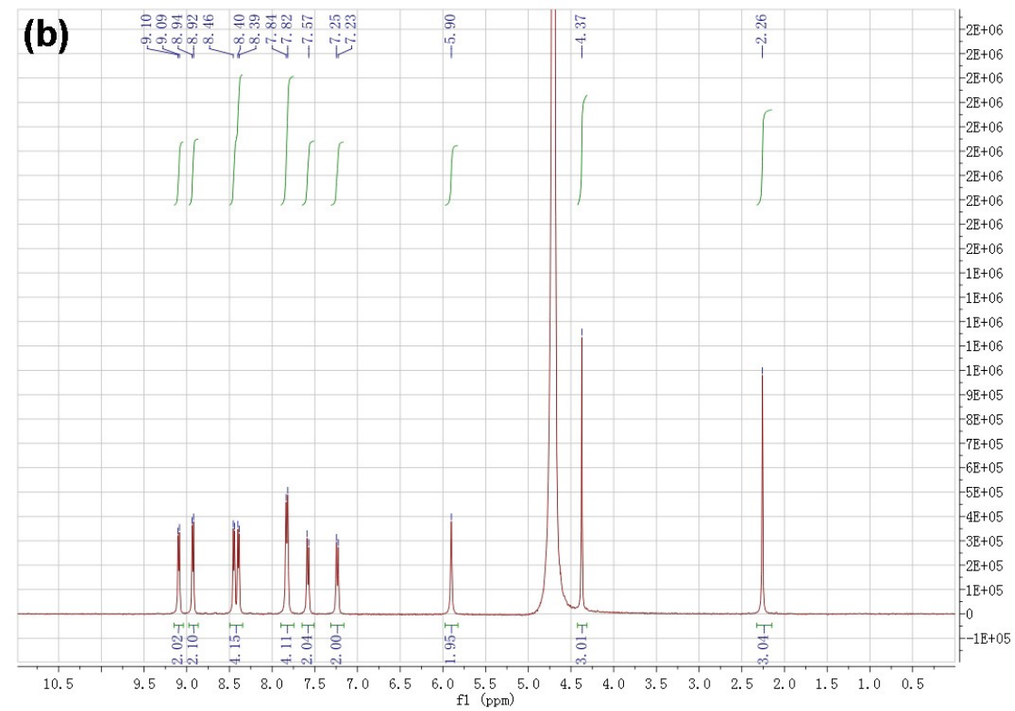
(b)
9.10
9.09
8.94
8.92
8.46
8.40
8.39
7.84
7.82
7.57
7.25
7.23
5.90
4.37
2.26
2.02
2.10
4.15
4.11
2.04
2.00
1.95
3.01
3.04
f1 (ppm)

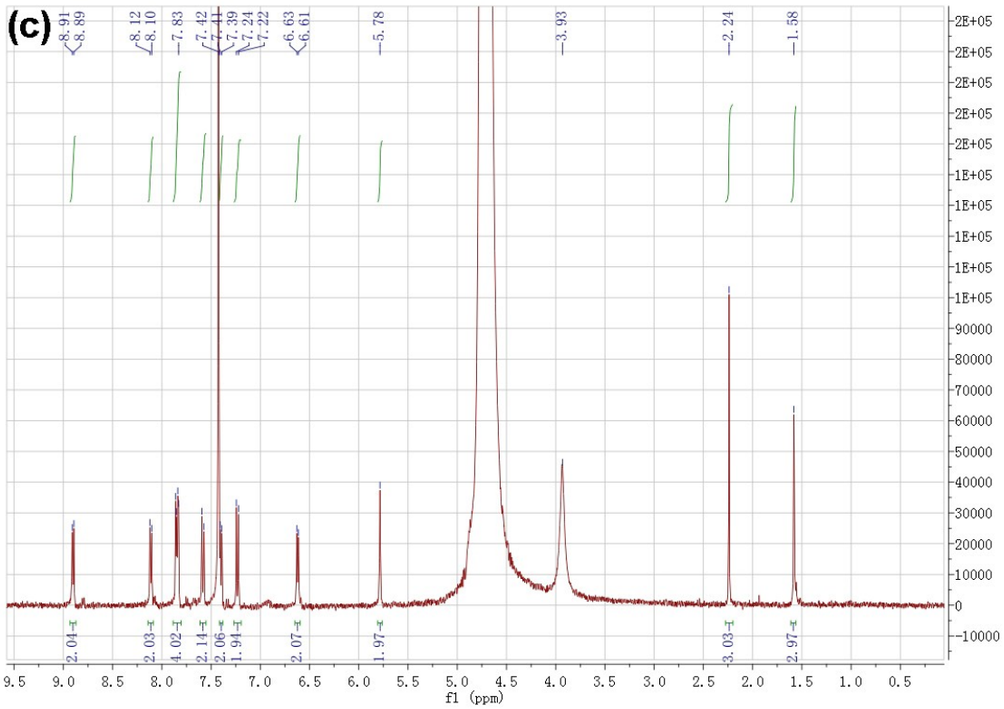

Supplementary Figure S18 | ^{1}H-NMR spectra (400MHz, D_2O, 298K) of SC_4, V^{2+}-*trans*-Az and SC_4: V^{2+}-*trans*-Az. (**a**) ^{1}H NMR spectrum of SC_4, (**b**) ^{1}H NMR spectrum of V^{2+}-*trans*-Az and (**c**) ^{1}H NMR spectrum of SC_4: V^{2+}-*trans*-Az.

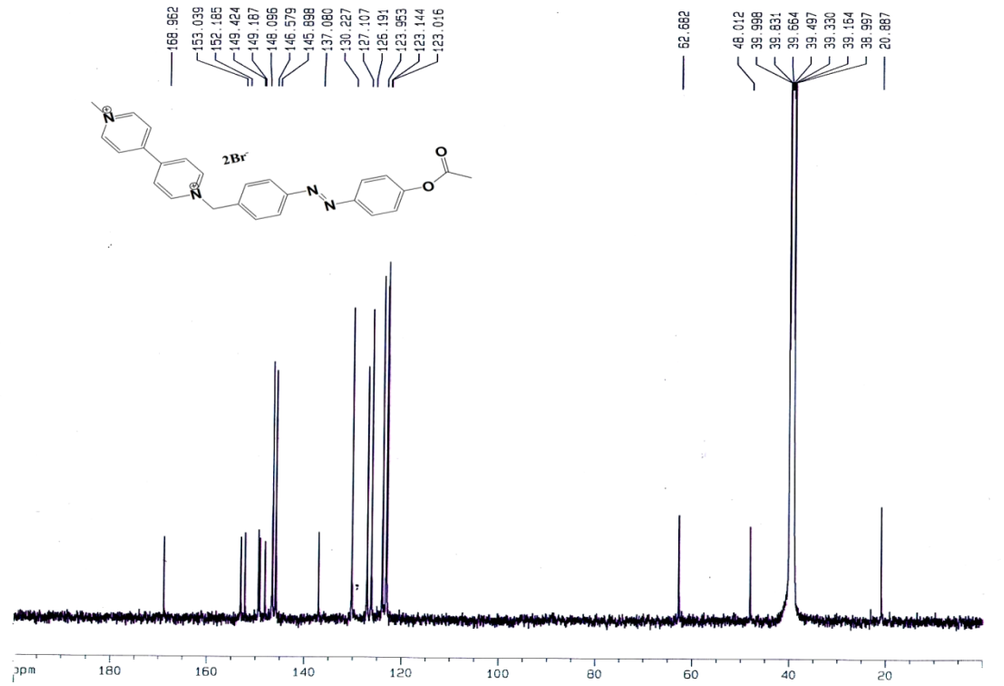

Supplementary Figure S19 | ^{13}C-NMR spectrum (400MHz, DMSO-d_6, 298K) of V^{2+}-*trans*-Az.

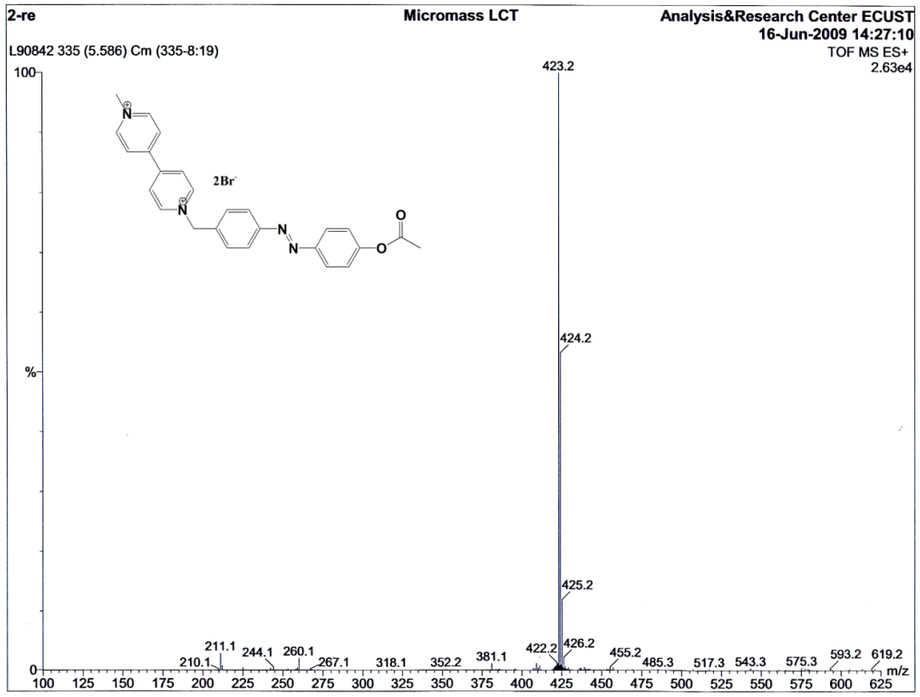

Supplementary Figure S20 | ESI-MS spectrum of V^{2+}-*trans*-Az.

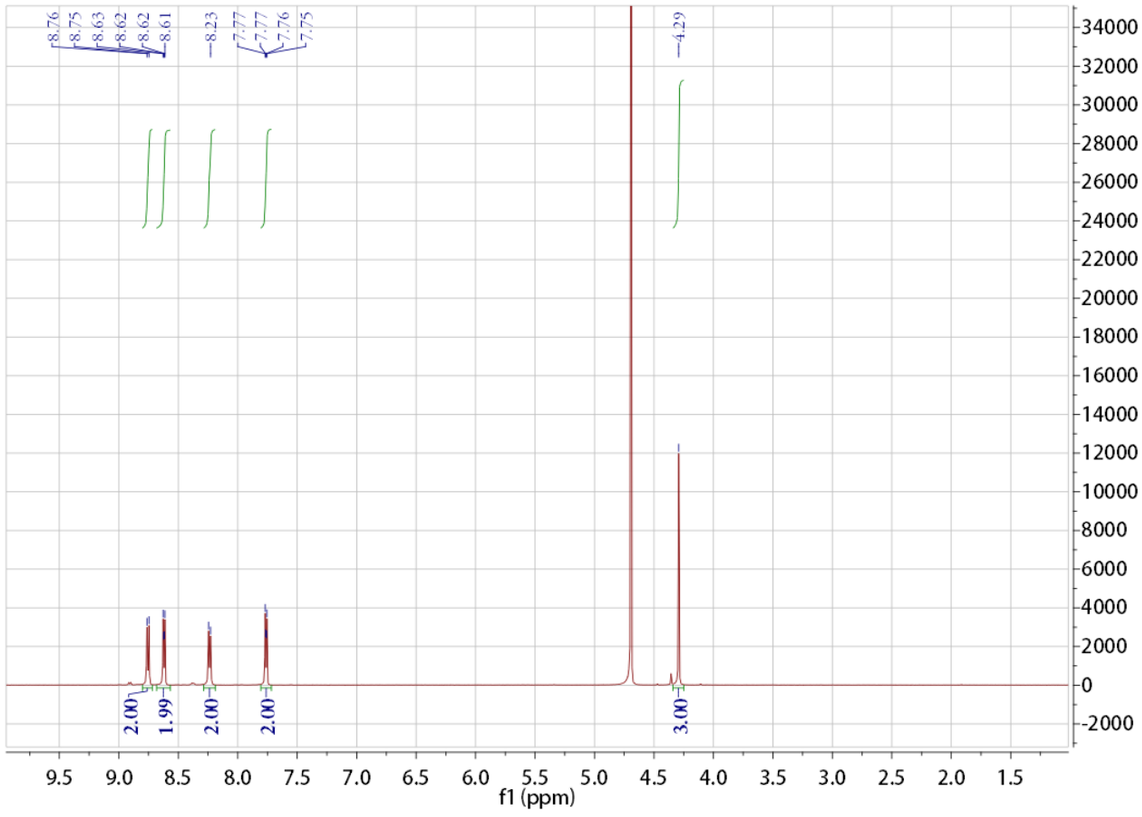

Supplementary Figure S21 | ^{1}H-NMR spectrum (400MHz, D_2O, 298K) of V^+.

Supplementary Reference

51. Matsumiya, H., Terazono, Y., Iki, N. & Miyano, S. Acid–base properties of sulfur-bridged calix [4] arenes. *J. Chem. Soc., Perkin Trans. 2*, 1166-1172 (2002).

52. Zhu, L. L., Zhang, D., Qu, D. H., Wang, Q. C., Ma, X., Tian, H. Dual-controllable stepwise supramolecular interconversions. *Chem. Commun.* **46,** 2587-2589 (2010).

53. Percec, V., Bera, T. K., De, B. B., Sanai, Y., Smith, J., Holerca, M. N., Barboiu, B., Grubbs, R. B., Frchet, J. M. J. Synthesis of functional aromatic multisulfonyl chlorides and their masked precursors. *J. Org. Chem.* **66,** 2104-2177 (2001).

54. Shinkai, S., Araki, K., Tsubaki, T., Arimura, T., Manabe, O. New syntheses of calixarene-*p*-sulphonates and *p*-nitrocalixarenes. *J. Chem. Soc., Perkin Trans. 1* 2297-2299 (1987).